Electronic Supplementary Information

2D Titanium Catecholate Metal-Organic Frameworks with Tunable Gas Adsorption and Ionic Conductivity

Yueting Li[a], Huanyu Liu[a], Lu Dai[a], Changli Wang[a], Jianning Lv[a], Xiangjian Meng[a], Anwang Dong[a], Bo Wang[a,b] and Pengfei Li[a]*

a Frontiers Science Center for High Energy Material, Key Laboratory of Cluster Science, Ministry of Education, Beijing Key Laboratory of Photoelectronic/Electrophotonic, Advanced Research Institute of Multidisciplinary Science, School of Chemistry and Chemical Engineering, Beijing Institute of Technology, Beijing, 100081, China

b Advanced Technology Research Institute (Jinan), Beijing Institute of Technology, Jinan, 250300, China

*E-mail: lipengfei@bit.edu.cn

Table of contents

Section 1. Materials and Characterization

All chemicals and solvents were purchased from commercial suppliers including J&K Scientific Co. Ltd., Energy Chemicals Co. Ltd., and Aladdin Reagent Co., Ltd, and used without further purification unless otherwise stated. Bis(acetylacetonato) titanium oxide (powder, 99.99% metal basis) was activated at 100 °C for 12 h under vacuum before use. Anhydrous solvents with molecular sieves were used throughout the experiments. Fourier transform infrared (FT-IR) spectra were collected in the range of 400-4000 cm^{-1} on Bruker ALPHA spectrometer. Powder X-ray diffraction (PXRD) was measured by a Rigaku MiniFlex 600 diffractometer operating at 40 kV voltage and 50 mA current with Cu-Kα X-ray radiation (λ = 0.154056 nm). ^{1}H NMR spectra were recorded on Bruker Ascend 400 MHz spectrometer. Solid-state ^{13}C CP/MAS NMR spectra were recorded on Bruker Avance 700 MHz spectrometer by using a 4 mm probe. All NMR measurements were performed at room temperature. X-ray photoelectron spectroscopy (XPS) was collected by using Thermo scientific ESCALAB 250Xi with Al Kα-radiation. Elemental analysis (EA) was conducted on a Vario EL-III elemental analyzer. The contents of Li, Na, K and Ti in Ti-DMTHA-M were determined by Prodigy7 inductively coupled plasma-atomic emission spectrometry (ICP-AES). Thermogravimetric analysis (TGA) was carried out on a NETZSCH Proteus thermal analyzer under a N_2 atmosphere at a heating rate of 10 °C/min within a temperature range of 30-800 °C. N_2 and CO_2 adsorptions were measured on Quantachrome instrument Autosorb-iQ at different temperatures after pretreatment at 120 °C under vacuum. The specific surface areas were calculated by the Brunauer-Emmett-Teller (BET) method. The pore size distributions were evaluated by the nonlocal density function theory (NLDFT). Transmission electron microscopy (TEM) images were collected on a JEOL JEM-2100F transmission electron microscope operating at 200 kV. Field emission scanning electron microscopes (FE-SEM) images were determined by JEOL model JSM-7500F. All electrochemical impedance spectroscopy tests were carried out on CHI 760E electrochemical workstation.

Section 2. Experimental Section

Synthesis of 9,10-dimethyl-2,3,6,7-tetramethoxyanthracene (DMTMA)

A mixture of veratrole (8 mL, 0.06 mol), methanol (5 mL, 0.12 mol), acetic acid (32 mL, 0.60 mol) and acetaldehyde in 40% water (12.5 mL, 0.22 mol) was added into an ice-cooled round-bottom flask and stirred for 5 min, then 32 mL of concentrated sulfuric acid were added dropwise over 15 min with continuous stirring. The reaction mixture turned from pink to dark purple during this process and then was stirred for 16 h at room temperature. The resulting mixture was then poured into a beaker full of crushed ice and the precipitate was filtered and washed with water and acetone to get an off-white solid. ^{1}H NMR (400 MHz, $CDCl_3$): δ = 7.4 (s, 4H), 4.08 (s, 12H), 2.95 (s, 6H).

Synthesis of 9,10-dimethyl-2,3,6,7-tetrahydroxyanthracene (DMTHA)

An oven-dried Schlenk flask loaded with DMTMA (1.63 g, 4.9 mmol) was evacuated and backfilled with Ar three times. Anhydrous dichloromethane (40 mL) was then added and stirred for 5 min. 1 M boron tribromide solution in dichloromethane (22 mL) was injected slowly into the suspension, the color turned from purple to brownish yellow after 2 h of continuous stirring. The sediment was filtered and washed with water and methanol then dried under a vacuum at 60 °C overnight. ^{1}H NMR (400 MHz, DMSO-d_6): δ = 9.4 (s, 4H), 7.34 (s, 4H), 2.70 (s, 6H).

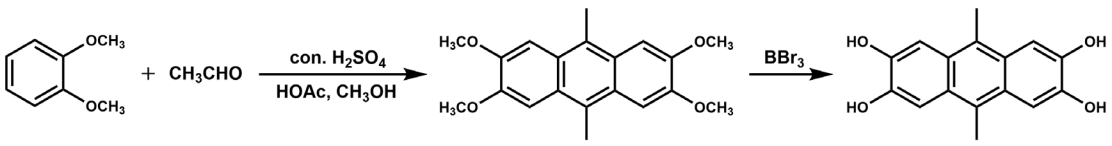

Scheme S1. The synthetic route of DMTHA.

Section 3 Supplementary figures

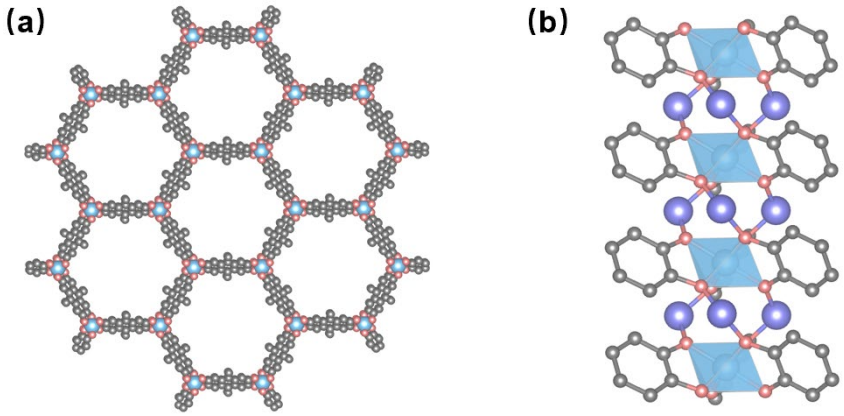

Figure S1. The structural models of Ti-DMTHA-M (a) top view and (b) side view. Grey, pink, blue, and purple spheres represent C, O, Ti, and counter ions, respectively.

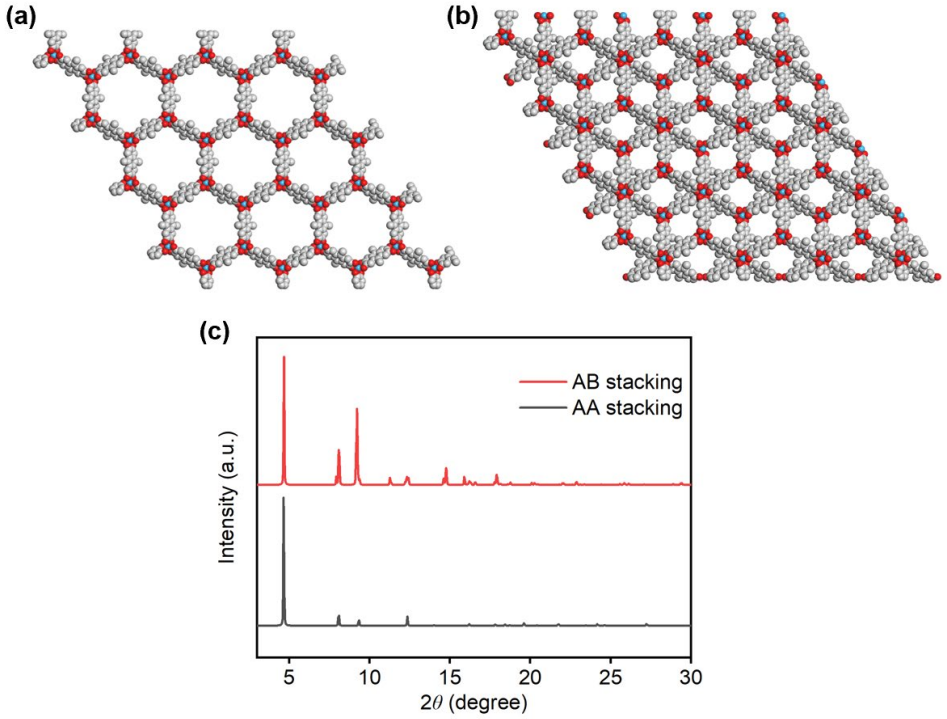

Figure S2. (a-b) The eclipsed AA stacking model and staggered AB stacking model of Ti-DMTHA-M, (c) the simulated PXRD patterns.

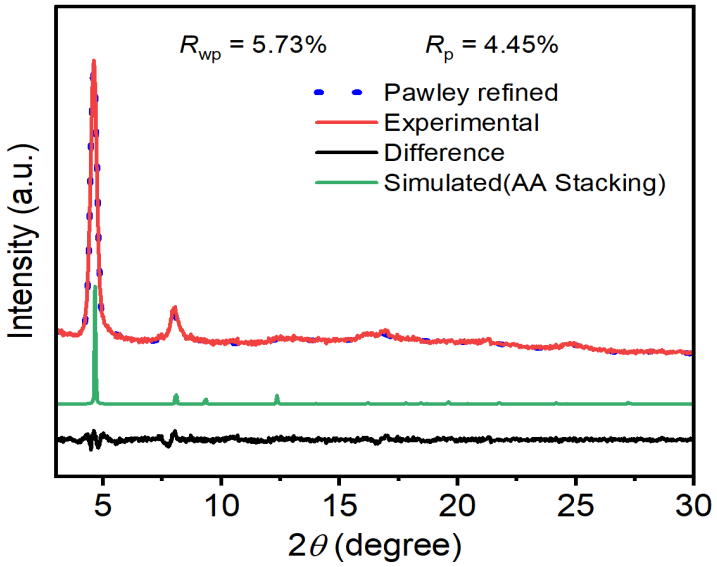

Figure S3. Experimental PXRD, Pawley refined PXRD, simulated PXRD, and the difference between experimental and Pawley refined PXRD of Ti-DMTHA-Li.

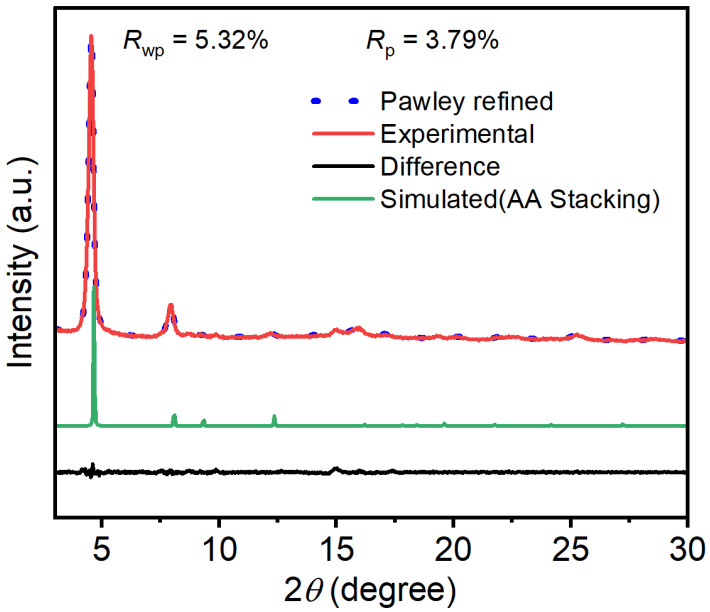

Figure S4. Experimental PXRD, Pawley refined PXRD, simulated PXRD, and the difference between experimental and Pawley refined PXRD of Ti-DMTHA-Na.

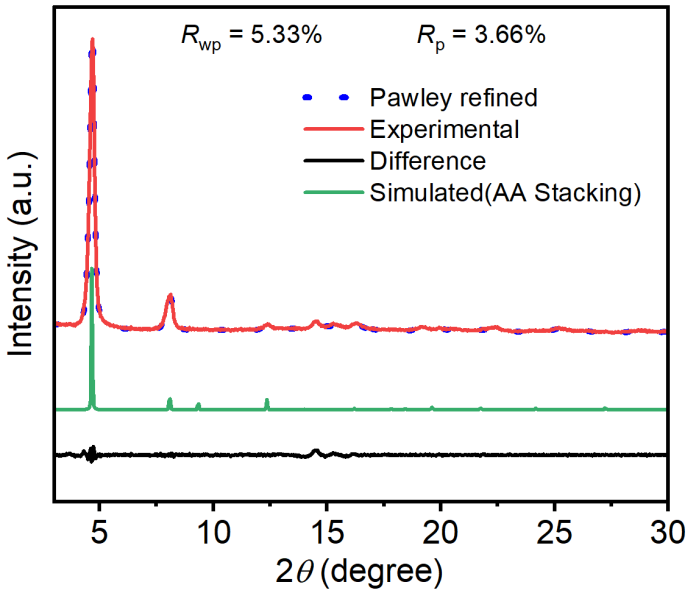

Figure S5. Experimental PXRD, Pawley refined PXRD, simulated PXRD, and the difference between experimental and Pawley refined PXRD of Ti-DMTHA-K.

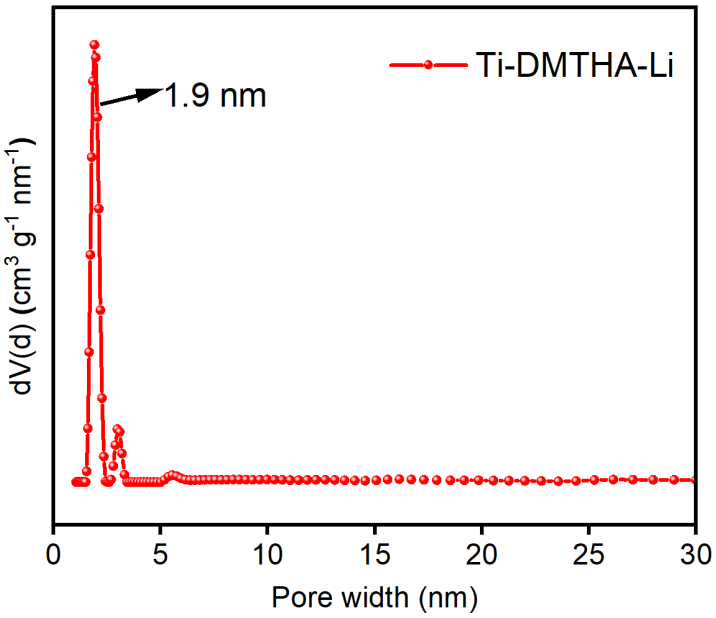

Figure S6. Pore size distribution of Ti-DMTHA-Li.

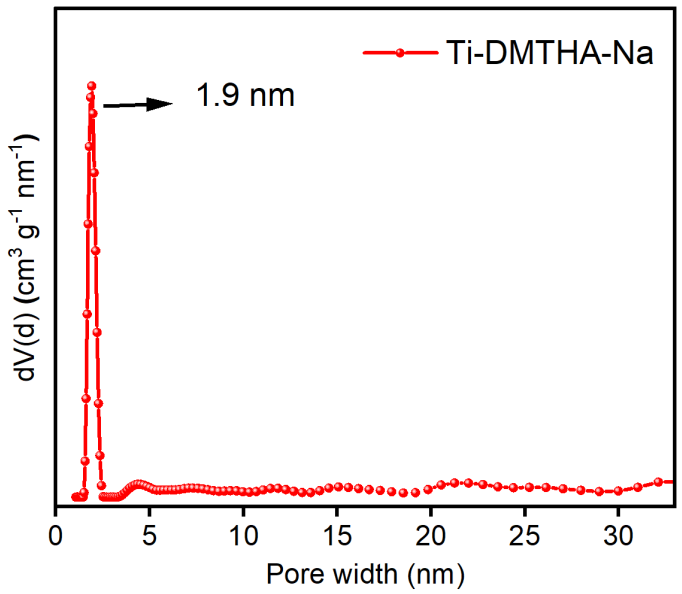

Figure S7. Pore size distribution of Ti-DMTHA-Na.

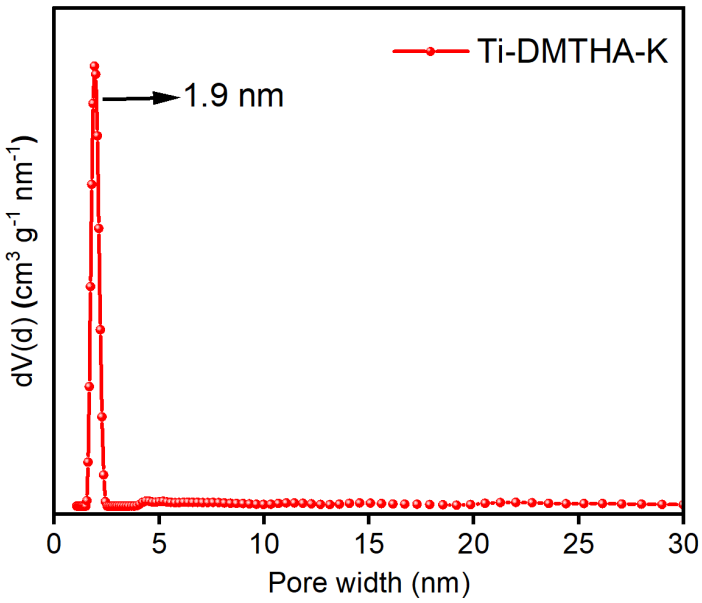

Figure S8. Pore size distribution of Ti-DMTHA-K.

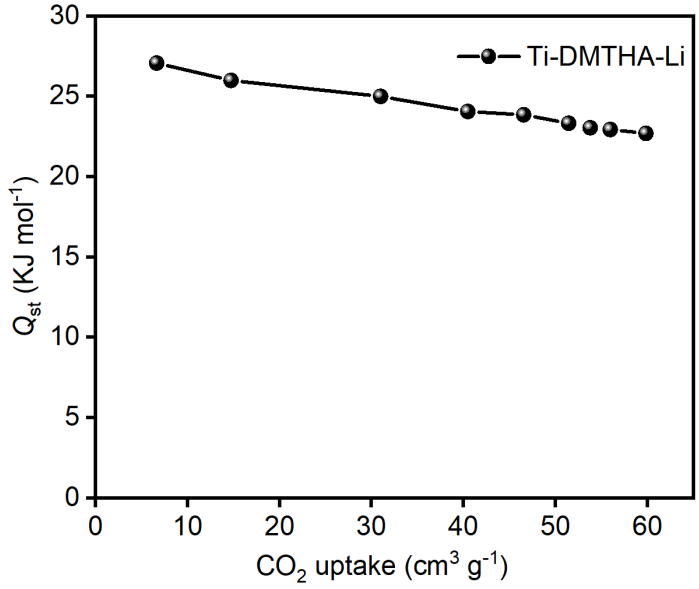

Figure S9. The isosteric heat of adsorption of Ti-DMTHA-Li.

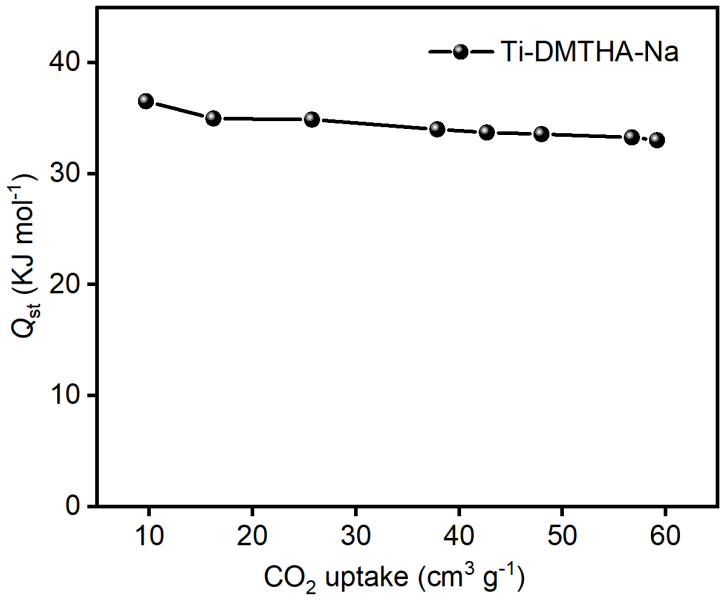

Figure S10. The isosteric heat of adsorption of Ti-DMTHA-Na.

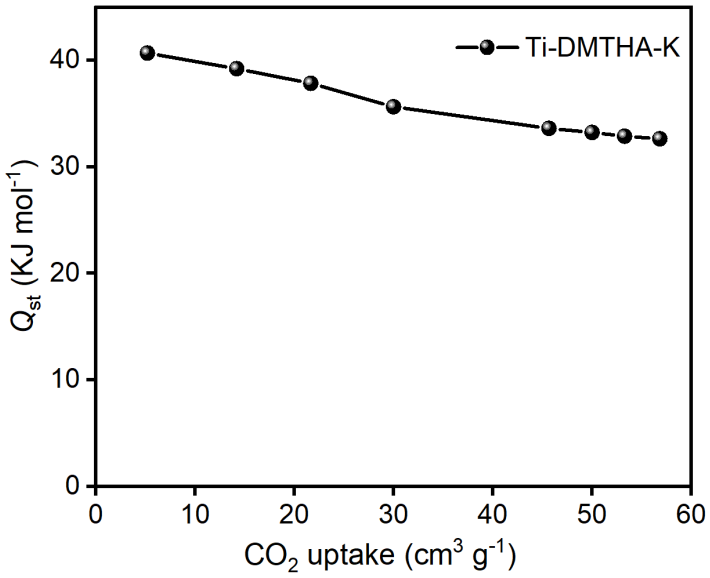

Figure S11. The isosteric heat of adsorption of Ti-DMTHA-K.

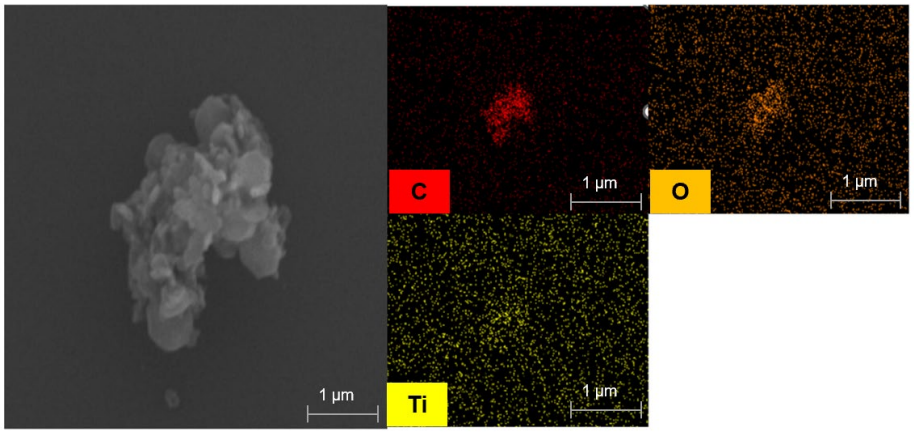

Figure S12. Energy dispersive spectroscopy mapping of Ti-DMTHA-Li.

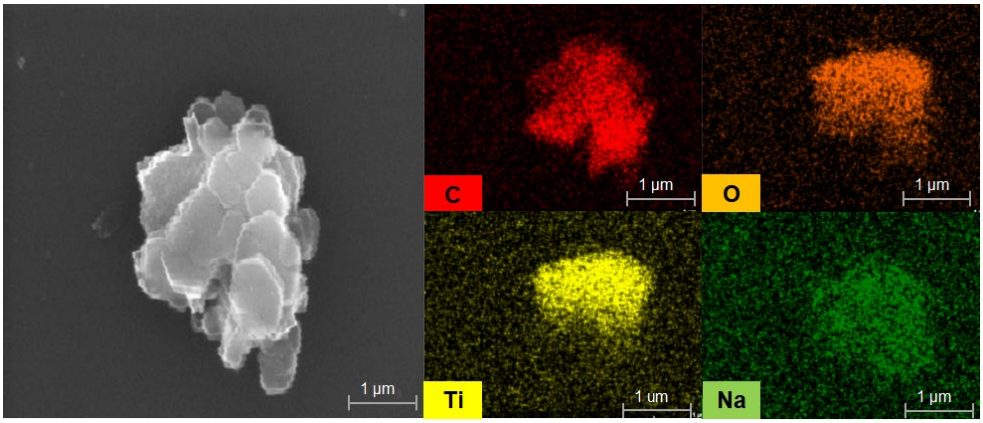

Figure S13. Energy dispersive spectroscopy mapping of Ti-DMTHA-Na.

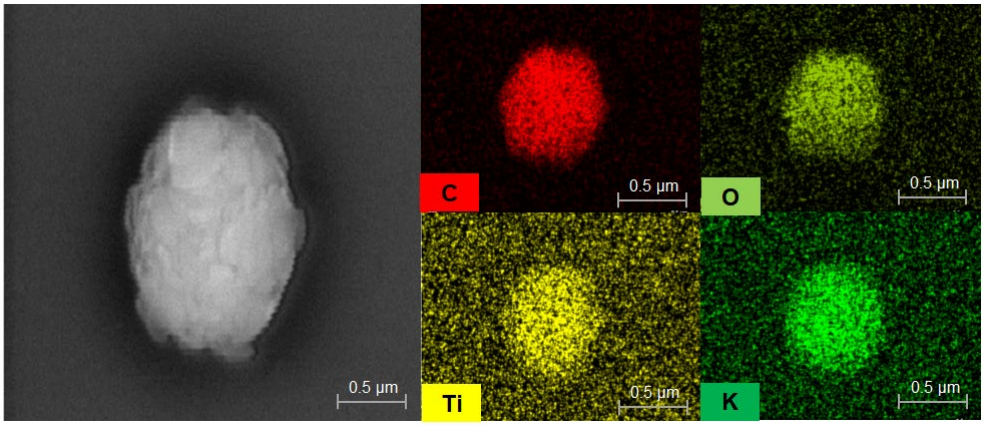

Figure S14. Energy dispersive spectroscopy mapping of Ti-DMTHA-K.

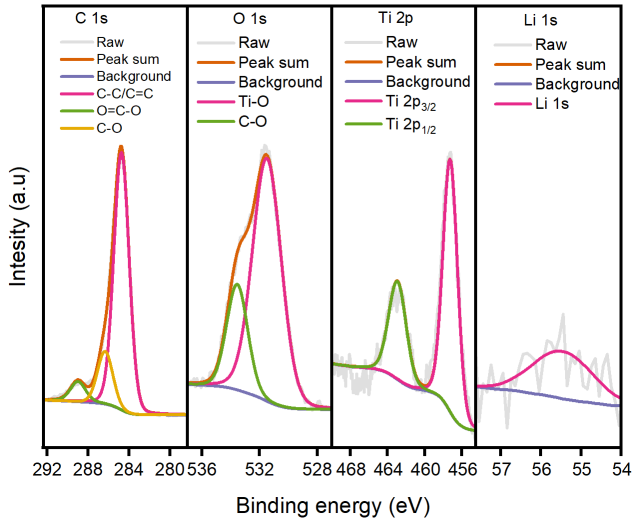

Figure S15. High-resolution XPS spectra of Ti-DMTHA-Li.

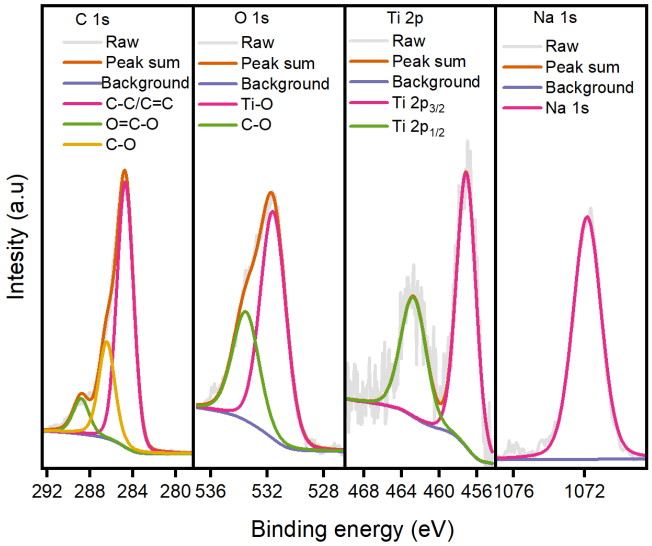

Figure S16. High-resolution XPS spectra of Ti-DMTHA-Na.

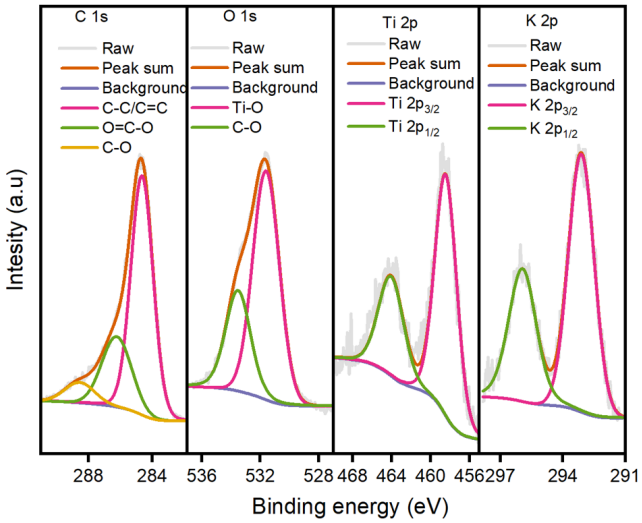

Figure S17. High-resolution XPS spectra of Ti-DMTHA-K.

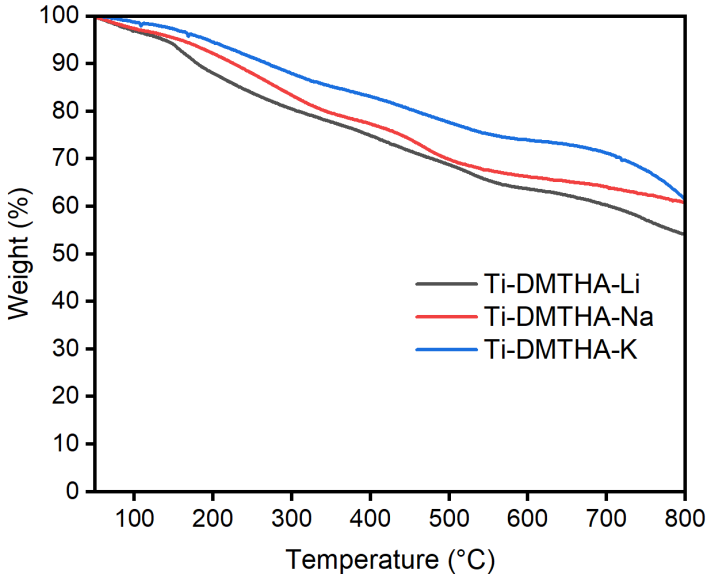

Figure S18. TGA comparison of Ti-DMTHA-Li, Ti-DMTHA-Na and Ti-DMTHA-K.

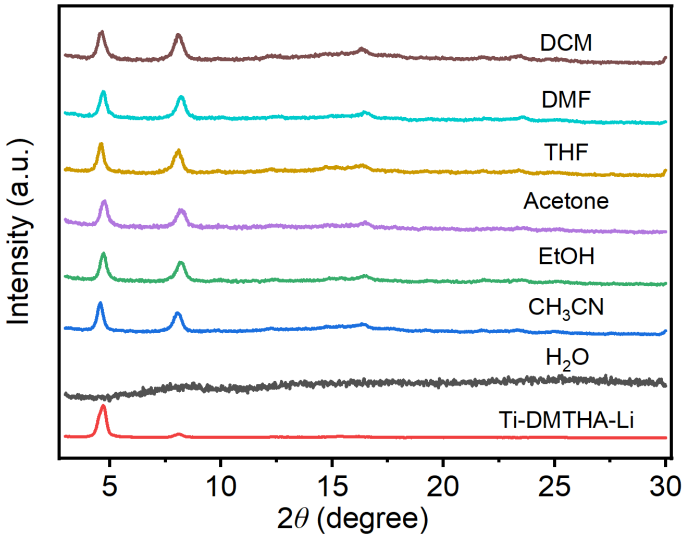

Figure S19. PXRD patterns of Ti-DMTHA-Li after immersing in different solvents for 24 h.

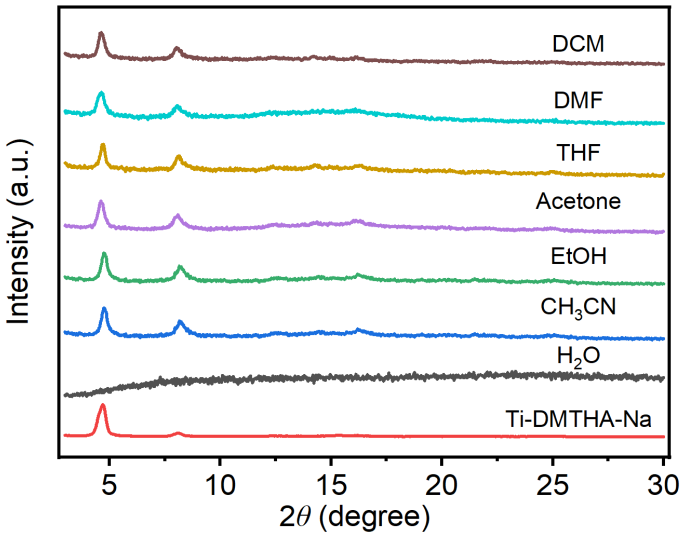

Figure S20. PXRD patterns of Ti-DMTHA-Na after immersing in different solvents for 24 h.

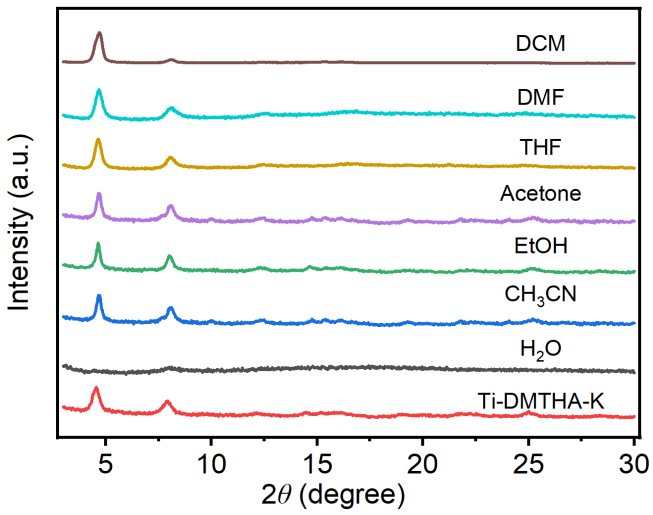

Figure S21. PXRD patterns of Ti-DMTHA-K after immersing in different solvents for 24 h.

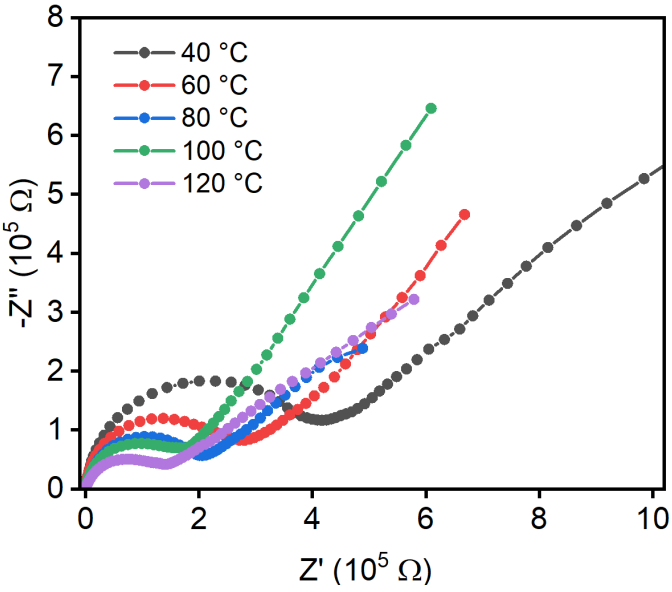

Figure S22. Nyquist plots of the pristine Ti-DMTHA-Li at different temperatures.

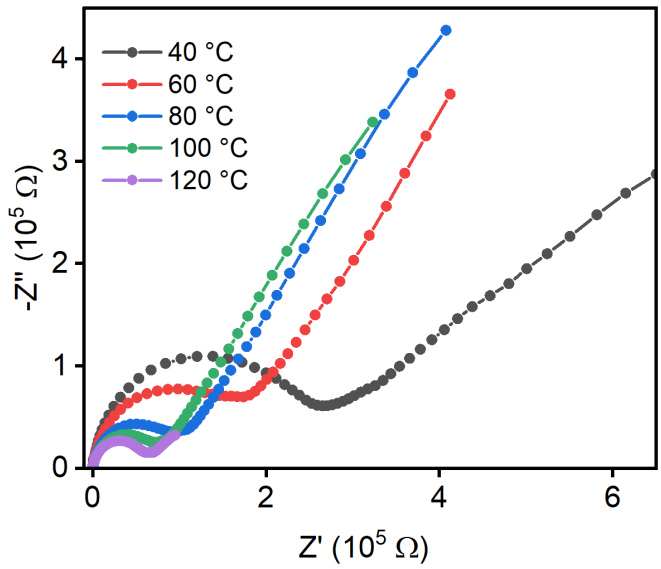

Figure S23. Nyquist plots of the pristine Ti-DMTHA-Na at different temperatures.

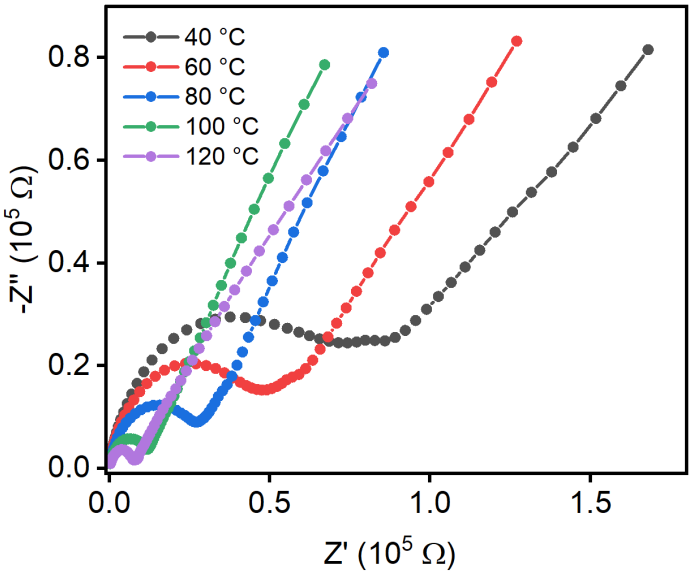

Figure S24. Nyquist plots of the pristine Ti-DMTHA-K at different temperatures.

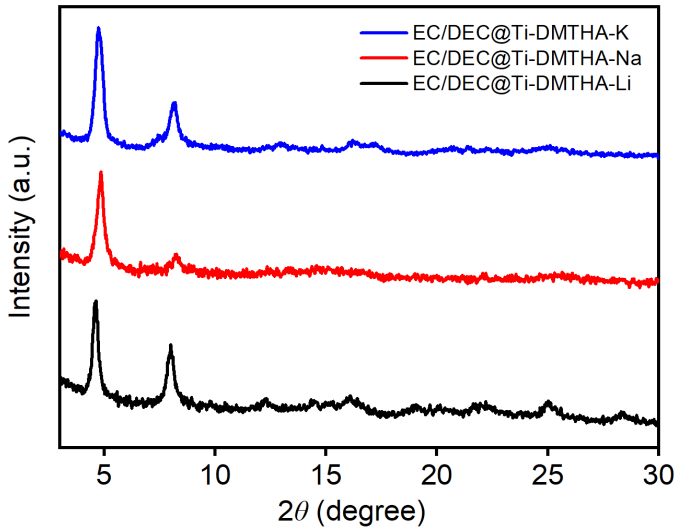

Figure S25. PXRD patterns of Ti-DMTHA-M after immersing in EC/DEC for 24 h.

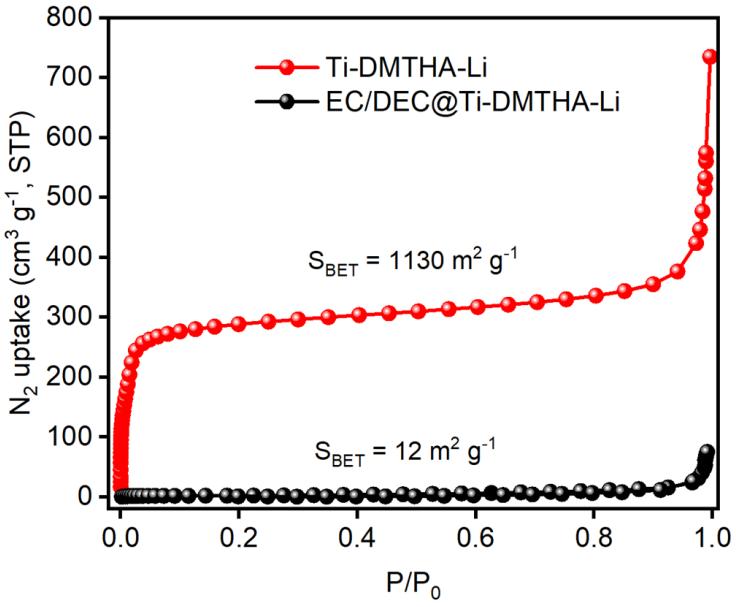

Figure S26. N_2 isotherms of Ti-DMTHA-Li and EC/DEC@Ti-DMTHA-Li.

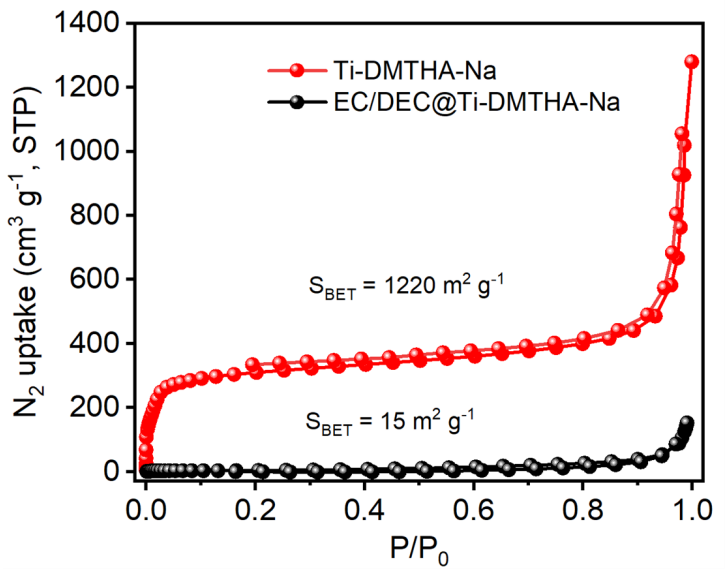

Figure S27. N_2 isotherms of Ti-DMTHA-Na and EC/DEC@Ti-DMTHA-Na.

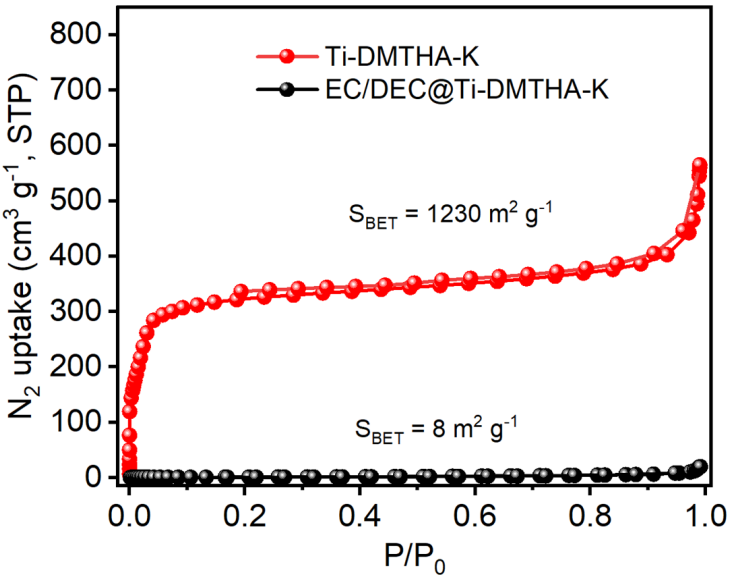

Figure S28. N_2 isotherms of Ti-DMTHA-K and EC/DEC@Ti-DMTHA-K.

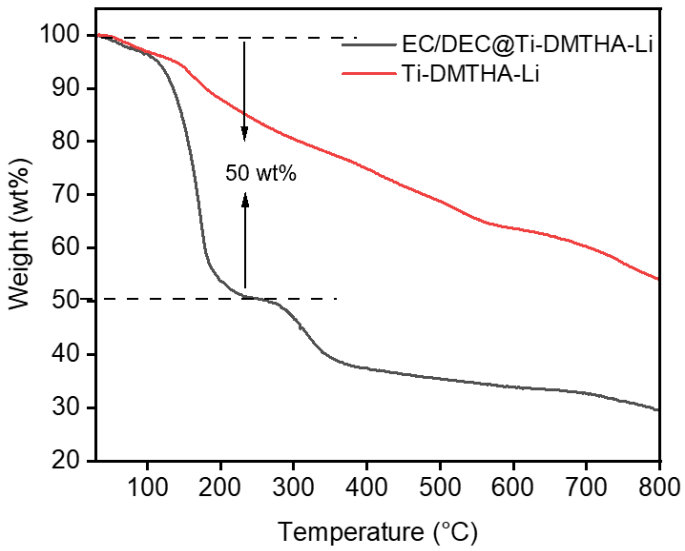

Figure S29. TGA comparison of Ti-DMTHA-Li and EC/DEC@Ti-DMTHA-Li.

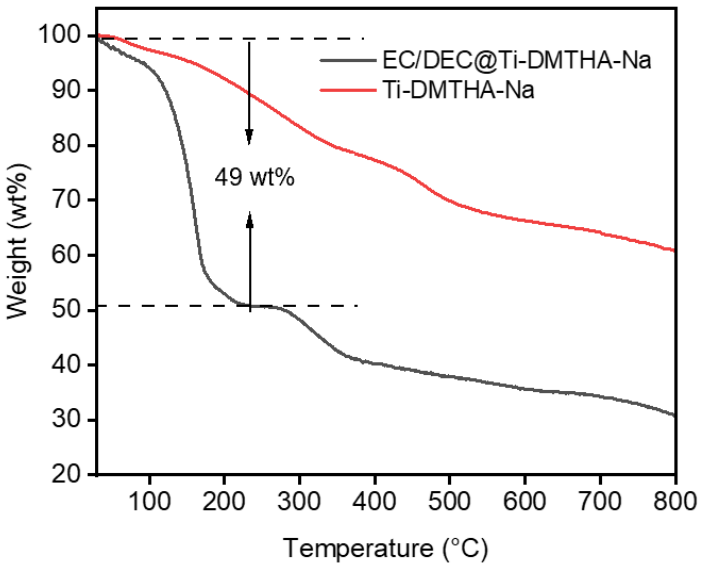

Figure S30. TGA comparison of Ti-DMTHA-Na and EC/DEC@Ti-DMTHA-Na.

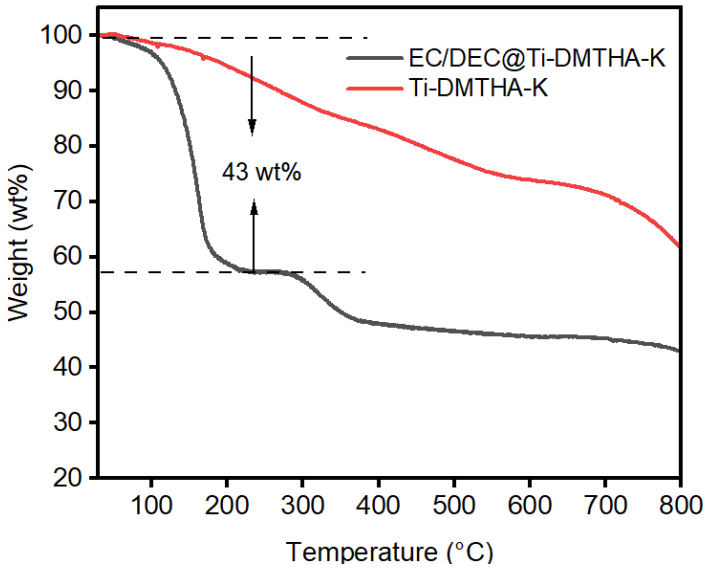

Figure S31. TGA comparison of Ti-DMTHA-K and EC/DEC@Ti-DMTHA-K.

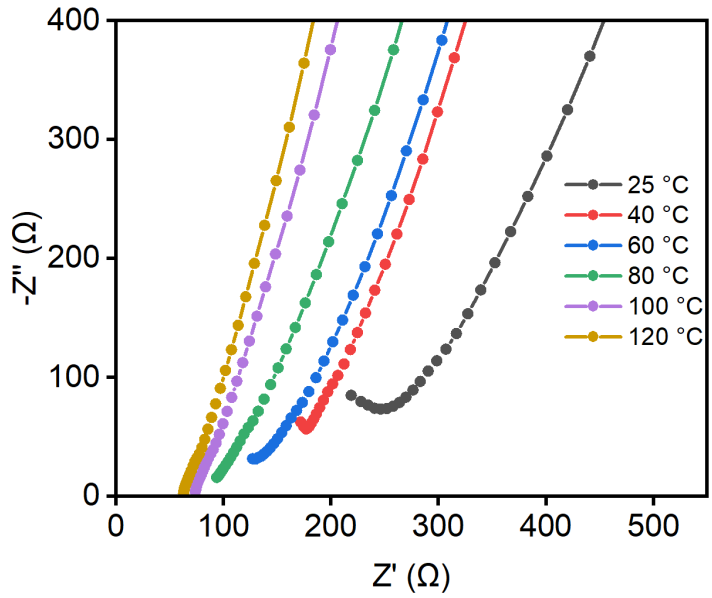

Figure S32. Nyquist plots of the $NaClO_4$@Ti-DMTHA-Na at different temperatures.

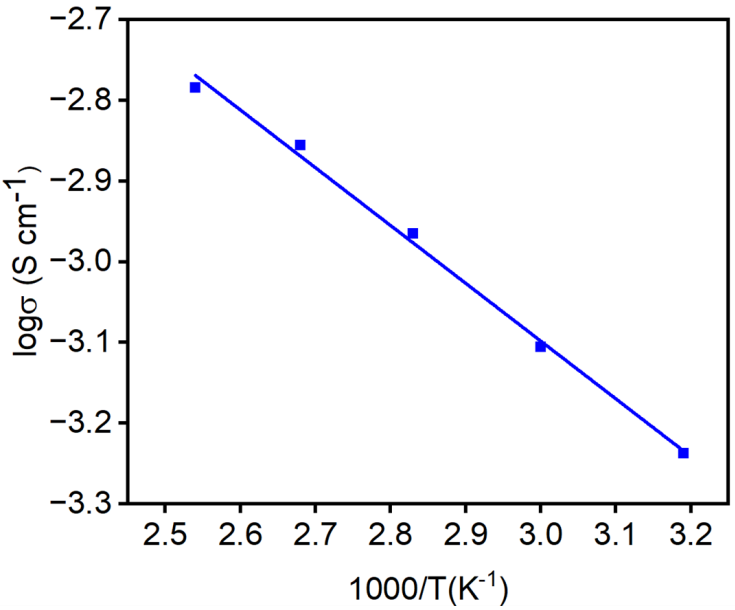

Figure S33. The Arrhenius plot of $NaClO_4$@Ti-DMTHA-Na.

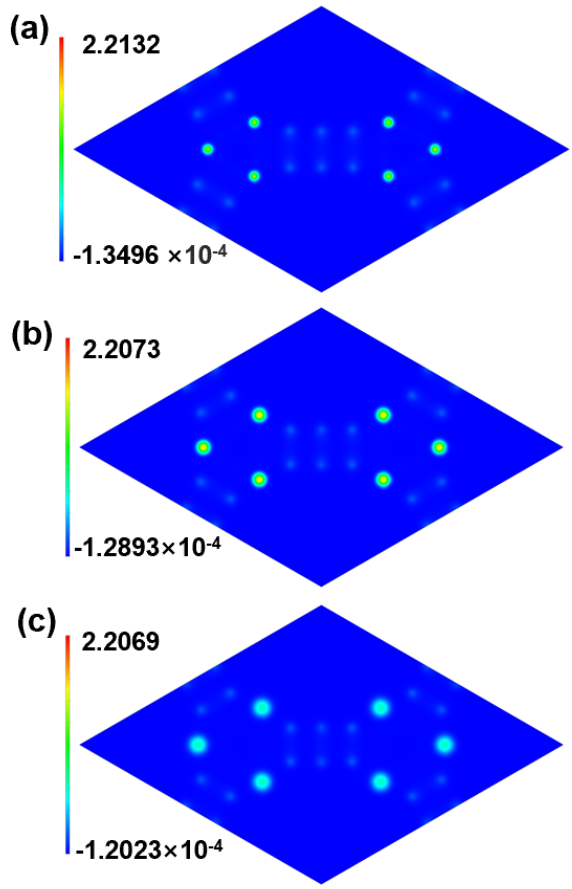

Figure S34. Two-dimensional electron density contour maps of (a) Ti-DMTHA-Li, (b) Ti-DMTHA-Na, and (c) Ti-DMTHA-K. The electron density decreases as the color changes from red to blue via green.

Section 4. Supplementary Tables

Table S1. The CO_2 adsorption comparison of MOF-based materials at 1 bar and 273 K.

Adsorbent	Capacity (mmol g^{-1})	Ref.
MAF-23	3.3	1
IFMC-1	4.1	2
MAF-66	6.3	3
NH_2-MIL-125	4.0	4
TMOF-1	2.2	5
LIFM-26	5.4	6
UiO-66-AD4	3.6	7
UiO-66-AD6	3.8	7
CPM-33b	7.8	8
CPM-33a	6.1	8
USTC-253	3.7	9
Zn-TAZ	1.2	10
$Cd_2(tp)_2(dptz)_2$·DMF	2.5	11
$Cu_3(pmtz)_6$·DMF	0.8	12
PyUiO-66	2.3	13
4-TPOM	2.8	14
PCN-224	3.9	15
PCN-224(Mg)	2.1	15
MOF-FNP-$MeOH_{0.3}$	4.0	16
MOF-DM-MeOH	4.2	16
MOF-FNP- MeOH	3.7	16
Ti-DMTHA-Li	**4.3**	**This work**
Ti-DMTHA-Na	**4.8**	**This work**
Ti-DMTHA-K	**4.9**	**This work**

Table S2. Calculated formula, elemental analysis, and ICP-AES results for Ti-DMTHA-M.

		C (%)	**H (%)**	**Ti (%)**	**M (%)**
$C_{26}H_{23}Li_2O_6Ti$	Calcd.	63.32	4.70	9.71	2.81
	Found	60.12	4.95	9.52	2.54
$C_{26}H_{23}Na_2O_6Ti$	Calcd.	59.45	4.41	9.11	8.75
	Found	58.90	4.10	8.82	8.10
$C_{26}H_{23}K_2O_6Ti$	Calcd.	56.01	4.16	8.59	14.03
	Found	54.83	4.17	8.12	13.45

Table S3. The comparison of MOF-based solid-state Na ion conduction materials.

MOF materials	Description	Conductivity ($S\ cm^{-1}$)	Ea (eV)	T (°C)	Ref.
EHUI(Sc, Na)	$NaBF_6$	9.2×10^{-5}	0.64	37	17
MIT-20(Na)	NaSCN	1.8×10^{-5}	0.39	25	18
MIL-100(Al)	$NaClO_4$	4.4×10^{-4}	0.28	RT	19
MIL-121	NaSCN	1.0×10^{-4}	0.36	25	20
S-IL@ZIF-8	Na-IL	2.0×10^{-4}	0.26	RT	21
UIOSNa	Na-IL	3.6×10^{-4}	—	RT	22
Ti-DMTHA-Na	EC/DEC	1.4×10^{-5}	0.22	40	**This work**
Ti-DMTHA-Na	$NaClO_4$	4.5×10^{-4}	0.15	25	**This work**

Note: PC = propylene carbonate, EC = ethylene carbonate, DEC = diethyl carbonate.

Section 5. Supplementary References

1. P. Q. Liao, D. D. Zhou, A. X. Zhu, L. Jiang, R. B. Lin, J. P. Zhang and X. M. Chen, *J. Am. Chem. Soc.*, 2012, **134**, 17380-17383.
2. J.-S. Qin, D.-Y. Du, W.-L. Li, J.-P. Zhang, S.-L. Li, Z.-M. Su, X.-L. Wang, Q. Xu, K.-Z. Shao and Y.-Q. Lan, *Chem. Sci.*, 2012, **3**, 2114-2118.
3. R. B. Lin, D. Chen, Y. Y. Lin, J. P. Zhang and X. M. Chen, *Inorg. Chem.*, 2012, **51**, 9950-9955.
4. S. N. Kim, J. Kim, H. Y. Kim, H. Y. Cho and W. S. Ahn, *Catal. Today*, 2013, **204**, 85-93.
5. G. Zhang, G. Wei, Z. Liu, S. R. J. Oliver and H. Fei, *Chem. Mater.*, 2016, **28**, 6276-6281.
6. C.-X. Chen, S.-P. Zheng, Z.-W. Wei, C.-C. Cao, H.-P. Wang, D. Wang, J.-J. Jiang, D. Fenske and C.-Y. Su, *Chem. Eur. J.*, 2017, **23**, 4060-4064.
7. D. H. Hong and M. P. Suh, *Chem. Eur. J.*, 2014, **20**, 426-434.
8. X. Zhao, X. Bu, Q.-G. Zhai, H. Tran and P. Feng, *J. Am. Chem. Soc.*, 2015, **137**, 1396-1399.
9. Z.-R. Jiang, H. Wang, Y. Hu, J. Lu and H.-L. Jiang, *ChemSusChem*, 2015, **8**, 878-885.
10. R. Das, S. S. Dhankhar and C. M. Nagaraja, *Inorg. Chem. Front.*, 2020, **7**, 72-81.
11. R. Zhang, J. H. Huang, D. X. Meng, F. Y. Ge, L. F. Wang, Y. K. Xu, X. G. Liu, M. M. Meng, Z. Z. Lu, H. G. Zheng and W. Huang, *Dalton Trans.*, 2020, **49**, 5618-5624.
12. R. Zhang, D. X. Meng, F. Y. Ge, J. H. Huang, L. F. Wang, Y. K. Xv, X. G. Liu, M. M. Meng, H. Yan, Z. Z. Lu, H. G. Zheng and W. Huang, *Dalton Trans.*, 2020, **49**, 2145-2150.
13. Y. L. Liu, Y. Di, F. Chen, C. Zhou and B. Liu, *Dalton Trans.*, 2021, **50**, 3848-3853.
14. G. Chakraborty, P. Das and S. K. Mandal, *Inorg. Chem.*, 2021, **60**, 5071-5080.
15. R. Das, S. S. Manna, B. Pathak and C. M. Nagaraja, *ACS Appl. Mater. Interfaces*, 2022, **14**, 33285-33296.
16. C. Wang, Z. Wang, J. Yu, K. Lu, W. Bao, G. Wang, B. Peng, W. Peng and F. Yu, *Chem. Eng. J.*, 2023, **454**, 140078.
17. J. Cepeda, S. Pérez-Yáñez, G. Beobide, O. Castillo, E. Goikolea, F. Aguesse, L. Garrido, A. Luque and P. A. Wright, *Chem. Mater.*, 2016, **28**, 2519-2528.
18. S. S. Park, Y. Tulchinsky and M. Dinca, *J. Am. Chem. Soc.*, 2017, **139**, 13260-13263.
19. S. Ma, L. Shen, Q. Liu, W. Shi, C. Zhang, F. Liu, J. A. Baucom, D. Zhang, H. Yue, H. B. Wu and Y. Lu, *ACS Appl. Mater. Interfaces*, 2020, **12**, 43824-43832.
20. G. Zhang, J. Shu, L. Xu, X. Cai, W. Zou, L. Du, S. Hu and L. Mai, *Nano-micro Lett.*, 2021, **13**, 105.
21. X. G. Yu, N. S. Grundish, J. B.Goodenough, A. Manthiram, *ACS Appl. Mater. Interfaces*, 2021, **12**, 24662-24669.
22. V. Nozari, C. Calahoo, J. M. Tuffnell, P. Adelhelm, K. Wondraczek, S. E. Dutton, T. D. Bennett and L. Wondraczek, *Sci. Rep.*, 2020, **10**, 3532.